

Biochemistry. Author manuscript; available in PMC 2011 November 2.

Published in final edited form as:

Biochemistry. 2010 November 2; 49(43): 9413–9423. doi:10.1021/bi101405y.

# Mechanistic studies of Agmatine Deiminase from multiple bacterial species<sup>†</sup>

Justin E. Jones  $^{1,2}$ , Christina J. Dreyton  $^{1,2}$ , Heather Flick  $^2$ , Corey P. Causey  $^2$ , and Paul R. Thompson  $^{1,2,*}$ 

- <sup>1</sup> Department of Chemistry, The Scripps Research Institute, Scripps Florida, 120 Scripps Way, Jupiter, Florida 33458
- <sup>2</sup> Department of Chemistry & Biochemistry, University of South Carolina, 631 Sumter Street, Columbia, SC 29208

#### Abstract

One subfamily within the guanidino-group modifying enzymes (GMEs) is the agmatine Deiminases (AgD). These enzymes catalyze the conversion of agmatine (decarboxylated arginine) to N-carbamoyl putrescine and ammonia. In plants, viruses, and bacteria, these enzymes are thought to be involved in energy production, biosynthesis of polyamines, and biofilm formation. In particular, we are interested in the role that this enzyme plays in pathogenic bacteria. Previously we reported the initial kinetic characterization of the agmatine deiminase from  $Helicobacter\ pylori$  and described the synthesis and characterization the two most potent inactivators AgD inactivators. Herein we have expanded our initial efforts to characterize the catalytic mechanisms of AgD from  $H.\ pylori$  as well  $Streptococcus\ mutans$ , and  $Porphromonas\ gingivalis$ . Through the use of pH rate profiles,  $pK_a$  measurements of the active site cysteine, solvent isotope effects, and solvent viscosity effects, we have determined that the AgDs, like PADs 1 and 4, utilize a reverse protonation mechanism.

The guanidino-group modifying enzymes (GMEs) are a large group of enzymes that catalyze a variety of reactions, including guanidinium hydrolysis and amidino group transfer (1). Family members include agmatine deiminase (AgD), amidinotransferase (AT), dimethylarginine dimethylaminohydrolase (DDAH), L-arginine deiminase (ADI), and protein arginine deiminase (PAD) (1). These enzymes all contain an active site Cys that plays a critical role in nucleophilic catalysis; nucleophilic attack on the guanidinium carbon generates an S-alkyl thiouronium intermediate that can either be hydrolyzed to generate a ureido group or transferred to an acceptor nucleophile (1).

In recent years, numerous studies have suggested that the dysregulation of individual GME family members is either associated with human disease or represent potential drug targets. Examples of the former include the gene encoding an AT in *Aphanizomenon ovalisporum*, a cyanobacteria, which is found in a genomic region that contains the genes encoding the enzymes thought to be responsible for the biosynthesis of cylindrospermopsin, a hepatotoxin. This data suggests that AT may play a role in the synthesis of this molecule (2); clindrospermopsin contains a guanidinium group that is thought to be generated via the actions of an AT. Another example is DDAH. This enzyme catalyzes the conversion of

<sup>&</sup>lt;sup>†</sup>This work was supported in part by the University Of South Carolina Research Foundation (P.R.T), TSRI Scripps Florida, and in part by NIH grant GM079357 to PRT.

<sup>\*</sup>To whom correspondence should be addressed: Department of Chemistry, The Scripps Research Institute, Scripps Florida, 130 Scripps Way, Jupiter, Fl, 33458 tel: (561)-228-2471; fax: (561)-228-2918; Pthompso@scripps.edu.

asymmetric dimethylarginine (ADMA) into citrulline. Dysregulated DDAH activity may contribute to the onset and progression of heart disease because ADMA acts as a competitive inhibitor of nitric oxide synthase, an enzyme that generates nitric oxide (NO), and is a key cellular messenger that regulates the cardiovascular system (3). Consistent with this possibility is the fact that the levels of ADMA are elevated in patients with heart disease. (3,4). Further consistent with this notion is the fact that a DDAH knockout mouse exhibits the hallmark symptoms of heart disease (5).

Potential drug targets among GME family members include the ADI in Gardia lamblia, which is the parasite responsible for causing giardiasis (i.e., beaver fever). In this organism, ADI metabolizes arginine to generate energy in the form of ATP, and siRNA knockdown experiments indicate that this enzyme is critical for parasite survival (6). Bacterial ADIs are also being investigated as potential therapeutics for the treatment of cancer (7). For example, in a recent Phase II study, patients with hepatocellular carcinoma were administered pegylated ADI (*Mycoplasma arginini*) and had a mean survival of 15.8 months; the estimated increase in survival time was 7.3 months (7). The PADs also represent potential drugs targets given the fact that their activity appears to be dysregulated in several human diseases, including cancer, multiple sclerosis, colitis, and rheumatoid arthritis (8).

In addition to the aforementioned GMEs, the AgDs, which catalyze the deimination of agmatine (i.e., decarboxylated arginine) to form *N*-carbamoyl putrescine (NCP) and ammonia (Figure 1), are potential drug targets. These enzymes are present in plants, bacteria, and viruses, where they are thought to play a role in energy generation, polyamine biosynthesis, and biofilm formation (9–12). In pathogenic bacteria (e.g. *Streptococcus mutans, Pseudomonas aeruginosa, and Helicobacter pylori*), these enzymes may also mediate acid resistance. However, in humans, agmatine is a cell signaling molecule involved in triggering a number of cellular processes (13–17), including the innate immune response. Thus, organisms that express agmatine degrading enzymes possess a potential mechanism to evade this component of the human immune system. A similar role for *H. pylori* arginase has also been proposed; the depletion of arginine attenuates the innate immune response (18). Given these putative roles in disease, many laboratories have become focused on developing inhibitors and chemical probes targeting individual members of this family (8,19–26).

To gain insights to aid inhibitor development, we and others initiated studies to characterize the catalytic mechanisms of a variety of GME family members, including a number of bacterial ADIs, DDAHs, as well as the PADs (1,6,27–29). Recently, we reported the purification, initial kinetic characterization, and structure of an AgD from *Helicobacter pylori*. Furthermore, site-directed mutagenesis verified that Cys324 is critical for catalysis and that Asp198 plays an important role in substrate recognition. Herein we describe detailed mechanistic studies on the *H. pylori* enzyme (HpAgD), as well as AgDs from *S. mutans* (SmAgD), a gram positive bacteria, and *P. gingivalis* (PgAgD), a gram negative bacteria. Note that while PgAgD is classified in genomic databases as a putative PAD, we show here that it is in fact an AgD, similar to our previous studies establishing that the *H. pylori* enzyme is an AgD (19).

We chose to focus on AgDs from these three organisms because (i) each of these organisms contains an AgD; (ii) the enzymes are readily expressed (10–30 mg/L media); and (iii) all three enzymes are expressed by pathogenic bacteria that are responsible for a number of human ailments including peptidic ulcers (*H. pylori*), tooth decay (*P. gingivalis*), and periodintitis and cardiovascular disease (*S. mutans*). In addition, these organisms metabolize agmatine differently. For example, *S. mutans* encodes a four gene operon known as *agu*BDAC that metabolizes agmatine into putrescine, ATP, ammonia, and carbon dioxide

(Figure 1). This system is thought to play a role in acid resistance and survival of the organism (11,30). On the other hand, *H. pylori* and *P. gingivalis* encode an AgD, but do not contain the four gene operon described above. Instead these bacteria contain an AgD that converts agmatine to NCP, which is then hydrolyzed to putrescine, ammonia, and CO<sub>2</sub> via NCP amidohydrolase (Figure 1).

The active site architecture of the GME superfamily has been shown to be highly conserved but the catalytic mechanisms vary between family members. For instance, PADs 1, 3, and 4 utilize reverse protonation mechanisms (28,29), while another enzyme in the same family, DDAH, has been suggested to use a substrate assisted mechanism (27). In the latter mechanism, substrate binds to the thiol form of the enzyme and the positive charge of the guanidinium depresses the thiol p $K_a$  such that the thiol proton is donated to solvent or an unknown base (Scheme 1; upper pathway). In contrast, in a reverse protonation mechanism, substrate binds preferentially to the thiolate form of the enzyme (Scheme 1; lower pathway). To aid our understanding of AgD catalysis, and address whether these enzymes use a substrate assisted or reverse protonation mechanism, we carried out detailed mechanistic studies on HpAgD, SmAgD, and PgAgD. Herein we report the results of pH rate profiles,  $pK_a$  measurements on the active site thiol, solvent isotope effects (SIEs), and solvent viscosity effects (SVEs). The results indicate that, like other GME hydrolases (1,6,27–29), these enzymes possess a high  $pK_a$  active site Cys, suggesting that these enzymes employ a reverse protonation mechanism. Furthermore, p $K_a$  measurements with N-(4-aminobutyl)-2fluoro-ethanimidamide (ABFA), a recently described AgD inhibitor (19), show that inactivation proceeds via a multistep mechanism that requires general acid catalysis.

#### **Materials and Methods**

#### Chemicals

Iodoacetamide and 2-chloroacetamidine were purchased from Oakwood Products (Columbia, SC). Dideuterium oxide was obtained from Cambridge Isotope Laboratories (Andover, MA). Agmatine sulfate was purchased from Sigma Aldrich (St. Louis, MO). ABFA and *N*-(4-aminobutyl)-2-chloro-ethanimidamide (ABCA) were synthesized as previously described (19).

#### Construction of an expression vector for SmAgD and PgAgD

S. mutans UA159 chromosomal DNA, which was the generous gift of Dr. Robert A. Burne (University of Florida), was used to amplify the SmAgD gene by PCR with the following primers: 5'-AAAAAACATATGGCAAAACGTATTAAAAATACAACTCC-3' and 5'-AAAAAACTCGAGTTAAGTTGCAGGTTGCTGTGTAATACAG-3'. The forward primer contains an NdeI restriction site (underlined) followed by 26 bases that correspond to the 5'-coding region of the SmAgD gene. The reverse primer contains an XhoI restriction site (underlined) followed by 31 bases that correspond to the 3'-coding region of SmAgD. The PCR amplified gene was then treated with NdeI and XhoI to facilitate cloning into the pET21 vector. The resulting pET21SmAgD construct was sequenced to ensure that no mutations were incorporated during the PCR amplification.

*P. gingivalis* W83 chromosomal DNA, which was obtained from Dr. Mary Ellen Davey (The Forsyth Institute, Boston, Ma), was used as the template to PCR amplify the gene encoding PgAgD with the following primers: 5′-

AAAAAACATATGACAAAGAGACTATTCCTGCCCGAATGGGC-3' and 5'-AAAAAACTCGAGTTAGCGTATGAATCCTTGGGGG-3'. The forward primer contains an *NdeI* restriction site (underlined) followed by 29 bases that correspond to the 5'-coding region of the PgAgD gene. The reverse primer contains an *XhoI* restriction site (underlined)

followed by 22 bases that correspond to the 3'-coding region of PgAgD. The PCR amplified gene was then treated with *Nde*I and *Xho*I to facilitate cloning of the PgAgD gene into the pET21 vector. The resulting pET21PgAgD construct was sequenced to ensure that no mutations were incorporated during the PCR amplification.

## Purification of HpAgD, SmAgD, and PgAgD

Both the *S. mutans* and *P. gingivalis* AgD enzymes were purified analogously to the method previously described for HpAgD (19). Briefly, the protein was recombinantly expressed, lysed by sonication, and then purified by a combination of anion exchange, heparin affinity, and size exclusion chromatography. Protein was  $\geq 95\%$  pure as assessed by SDS-PAGE. Protein was stored at -80 °C and was stable for  $\geq 6$  months.

## **Kinetic Assay**

A discontinuous assay that measures ureido-containing compounds was used to measure HpAgD, SmAgD and PgAgD activity (31,32). Briefly, ureido groups produced during the reaction (i.e., NCP) react with diacetyl monooxime under strongly acidic conditions to generate a chromophore that absorbs at 540 nm. Comparison of these absorbance values to a standard curve was used to quantify NCP product formation. The steady state kinetic parameters were determined by pre-incubating varying amounts of agmatine in 50 mM 4-(2-hydroxyethyl)-1-piperazineethanesulfonic acid (HEPES) pH 8.0 in a final volume of 60  $\mu$ L prior to the addition of enzyme to initiate the reaction. Reactions were allowed to proceed for either 10 min (HpAgD, PgAgD) or 6 min (SmAgD) at 37 °C. Enzyme activity was linear with respect to both time and enzyme concentration. Standard errors were typically less than 20%. Initial rates were fit by non-linear least fit squares to eq 1,

$$v=V_{\max}[S]/(K_m+[S]), \tag{1}$$

using the GraFit<sup>TM</sup> version 5.0.11 software package (33).

#### pH Studies

pH profiles were generated for HpAgD, PgAgD, and SmAgD by measuring the initial rates over a range of pH values (5.5–9.5) in 50 mM 2-(bis(2-hydroxyethyl)amino)-2-(hydroxymethyl)propane-1,3-diol (Bis-Tris) (pH 5.5–7.0), HEPES (pH 7.0–8.75), and *N*-cyclohexyl-2-aminoethanesulfonic acid (CHES) (pH 8.75–9.5) in the presence of various concentrations of agmatine (0–5 mM). The initial rates were fit to eq 1, and the  $k_{\rm cat}$  and  $k_{\rm cat}$ /  $K_{\rm m}$  values obtained for each pH value were then plotted versus pH, and fit to either eq 2 for PgAgD and SmAgD or eq 3 for HpAgD ( $k_{\rm cat}$  data only),

$$y=Y_{max} - Log(1+K_2/K_1+H/K_1+K_2/H),$$
 (2)

$$y=Y_{max}+Log(1+H/K_2)-Log(1+H/K_1),$$
 (3)

using GraFit version 5.0.11 (33).  $Y_{max}$  corresponds to the activity at the pH optimum. Note that an overlapping buffer scheme was used to ensure that alterations in the kinetics are not due to buffer effects. Specifically,  $k_{cat}$  and  $k_{cat}/K_m$  values were determined at pH 7.0 and 8.75 in two different buffers and the data were averaged; the values were in agreement between the two buffers. Also note that at each of the pH values tested, time course

experiments were performed and were linear for ≥15 min. For these experiments, buffer and substrate were pre-incubated for 10 min and the reaction was initiated by the addition of enzyme. Aliquots were taken at 0, 2, 4, 6, 10, and 15 min and the reaction was quenched by flash freezing in liquid nitrogen. Product formation was measured as described above.

#### **lodoacetamide Inactivation Experiments**

For SmAgD, 2  $\mu$ M of enzyme was incubated at 37 °C with an Inactivation Mix containing 50 mM HEPES (pH 7.0–9.0) and varying concentrations of iodoacetamide (0–20 mM). At different time points from 0–30 min, aliquots were removed from the Inactivation Mix, and subsequently added to a Reaction Mix (50 mM HEPES pH 8, 5 mM  $\beta$ -mercaptoethanol (to quench the iodoacetamide), and 5 mM agmatine) to measure residual AgD activity. This reaction proceeded for 15 min, and was quenched in liquid nitrogen. Product formation was then quantified using the methodology outlined above. For each iodoacetamide concentration, data were fit to eq 4,

$$v = v_o e^{-kt} \tag{4}$$

using GraFit version 5.0.11 (33). v is the velocity,  $v_o$  is the initial velocity, k is the pseudo-first order rate constant (i.e.,  $k_{obs}$ ), and t is time. Plots of the observed inactivation rates ( $k_{obs}$ ) versus inactivator concentration were linear and fit to eq 5,

$$k_{\text{obs}} = (k_{\text{inact}}/K_{\text{I}}) * [I]$$
(5)

where  $k_{\text{inact}}$  is the maximal inactivation rate,  $K_{\text{I}}$  is the concentration that yields half maximal inactivation, and [I] is the concentration of inactivator. The slopes of these plots, which correspond to  $k_{\text{inact}}/K_{\text{I}}$ , were then plotted versus pH and fit to eq 6,

$$y = ((Y_{min} + Y_{max}) * 10^{(pH-pKa)})/(10^{(pH-pKa)} + 1)$$
(6)

using GraFit version 5.0.11.  $Y_{min}$  and  $Y_{max}$  correspond to the minimum and maximum rates of inactivation, respectively.

For HpAgD, time course experiments in the absence and presence of increasing concentrations of iodoacetamide were performed over a range of pH values (pH 7.50–9.25). For these assays, 0.5 mM agmatine (dissolved in 50 mM HEPES) was incubated with various concentrations of iodoacetamide (0–20 mM) for 10 min at 37 °C. Subsequently, HpAgD was added to initiate the reaction. Aliquots (60  $\mu$ L) were taken at different time points (0, 2, 4, 6, 8, 10, 15 and 20 min) and quenched by flash freezing in liquid nitrogen. NCP production was quantified using the methodology outlined above and plotted versus time. The data were subsequently fit to eq 7,

$$[P] = v_i [1 - \exp^{(-kobs(app)*t)}]/k_{obs(app)}, \tag{7}$$

using GraFit version 5.0.11. P corresponds to the quantity of NCP produced during the reaction,  $v_i$  is the initial velocity,  $k_{\text{obs(app)}}$  is the apparent pseudo first order rate constant for enzyme inactivation, and t corresponds to time. To obtain  $k_{\text{obs}}$  values, the  $k_{\text{obs(app)}}$  values

were subsequently extrapolated to zero substrate concentration using the transformation described by eq 8,

$$1+[S]/K_{\rm M}$$
. (8)

The second order rate constants for the inactivation of HpAgD by iodoacetamide, i.e.  $k_{\text{inact}}/K_{\text{I}}$ , were then determined by plotting  $k_{\text{obs}}$  versus iodoacetamide concentration and fitting the data to eq 5 using Grafit version 5.0.11. The slopes of these plots, which correspond to  $k_{\text{inact}}/K_{\text{I}}$ , were then plotted versus pH and fit to eq 6.

#### 2-Chloroacetamidine Inactivation Experiments

The 2-chloroacetamidine inactivation experiments were performed essentially as described above. For SmAgD, inactivation mixtures, containing 50 mM HEPES (pH 7.0–9.0), were incubated with 2  $\mu$ M SmAgD and incubated for 10 min at 37 °C. Various concentrations of 2- chloroacetamidine (0–1 mM) were then added and aliquots at various time points (0–30 min) were removed, and added to Reaction Mixture containing 5 mM agmatine. The data was processed as described above.

For HpAgD, various concentrations of 2-chloroacetamidine (0–60 mM) were pre-incubated with 0.5 mM agmatine in 50 mM HEPES (pH 7.50–9.25) for 10 min at 37 °C. Reactions were then initiated by the addition of HpAgD and 60  $\mu$ L aliquots taken at different time points (0, 2, 4, 6, 8, 10, 15 and 20 min). Reactions were quenched by flash freezing in liquid nitrogen. NCP levels were quantified using the methodology outlined above and the pseudo first order rate constants for enzyme inactivation were determined. Because saturation was observed in the plots of  $k_{\rm obs}$  versus [I], the data were fit to eq 9,

$$k_{\text{obs}} = k_{\text{inact}}[I]/(K_I + [I]),$$
 (9)

using the GraFit<sup>TM</sup> version 5.0.11 software package.  $k_{\text{inact}}$  corresponds to the maximal rate of inactivation and  $K_{\text{I}}$  is the concentration of I that yields half-maximal inactivation.  $k_{\text{inact}}/K_{\text{I}}$ , was then plotted versus pH and fit to eq 6.

#### **Substrate Protection**

To evaluate the ability of substrate to protect against iodoacetamide and 2-chloroacetamidine induced inactivation, progress curves were generated with and without inactivator (50 mM iodoacetamide or 2-chloroacetamadine) at two different concentrations of substrate. For iodoacetamide, concentrations of 0.25 mM (8 ×  $K_{\rm m}$  for HpAgD and 2 ×  $K_{\rm m}$  for SmAgD) and 5 mM (170 ×  $K_{\rm m}$  for HpAgD and 13 ×  $K_{\rm m}$  for SmAgD) agmatine were used. For 2-chloroacetamadine, concentrations of 0.5 mM (17 ×  $K_{\rm m}$  for HpAgD and 2 ×  $K_{\rm m}$  for SmAgD) and 2 mM (67 ×  $K_{\rm m}$  for HpAgD and 5 ×  $K_{\rm m}$  for SmAgD) agmatine were used. Assay buffer was pre-incubated for 10 min at 37 °C and either HpAgD or SmAgD was added to initiate the reaction. Aliquots (60 µL) were taken at 0, 2, 4, 6, and 10 min and data analysis performed as described above.

#### **ABFA Inactivation**

ABFA inactivation experiments were performed using the methodology outlined above for the iodoacetamide and 2-chloroacetamide inactivation experiments. Briefly, various concentrations of ABFA (0–1 mM) were pre-incubated with 0.5 mM agmatine in 50 mM HEPES (pH 7.0–9.0) for 10 min at 37 °C. Reactions were then initiated by the addition of

SmAgD and aliquots (60  $\mu$ L) were removed at specific time points (0, 1, 2, 3, 4, 5 and 6 min). Reactions were quenched by flash freezing in liquid nitrogen. NCP levels were quantified using the methodology outlined above and the apparent pseudo first order rate constants for enzyme inactivation were determined. Saturation was observed only at the pH optimum (pH = 8) and the  $k_{\text{obs}}$  versus [I] data were fit to eq 8 using the GraFit<sup>TM</sup> version 5.0.11 software package. For all other pH values, the data were fit to eq 5.  $k_{\text{inact}}/K_{\text{I}}$ , was then plotted versus pH and fit to eq 6.

#### Solvent Isotope and Solvent Viscosity Effects

All buffers and solution were prepared in  $D_2O$ . Buffer pD values were determined using the following formula, pD = pH + 0.4. Reactions were performed in 50 mM Bis-Tris (pL 6.0–6.5), Tris (pL 7.0–8.5), CHES (pL 8.5) in the presence of various concentrations of agmatine (0.0–2.5 mM) in >95%  $D_2O$ . Reactions were performed and analyzed as described above. Solvent viscosity experiments were performed in 50 mM HEPES pH 8.0 and various concentrations of agmatine (0.0–2.5 mM) in 0, 10, 20, 25, and 30 % glycerol. The relative viscosity was measured using a Cannon Manning Semi-Micro Viscometer size 50 (Cannon Instrument CO.). Data analyses were performed as described above.

# IC<sub>50</sub> Determination

The  $IC_{50}$  values of ABFA and ABCA were determined for SmAgD and PgAgD as previously described (19). Varying concentrations of inhibitor were pre-incubated with enzyme in 50 mM HEPES pH 8 for 15 min at 37 °C. Agmatine (0.5 mM) was added and allowed to react for 15 min. The reaction was quenched by flash freezing in liquid nitrogen and product was measured as described above. Rates were fit to eq 10,

Fraction Activity=
$$1/(1+([I]/IC_{50}))$$
, (10)

using GraFit (version 5.0.11) (33), where [I] is the concentration of inhibitor, and  $IC_{50}$  is the concentration of inhibitor that yields half-maximal activity.

#### Results

#### pH Studies

In an effort to identify the optimal pH for AgD activity, as well as to begin to characterize the catalytic mechanism of these enzymes, pH profiles were constructed for HpAgD, SmAgD, and PgAgD by determining the steady state kinetic parameters of agmatine deimination over a range of pH values (5.0 to 10.0). The plots of log  $k_{\rm cat}/K_{\rm m}$  versus pH (Figure 2) are bell-shaped for all three enzymes, suggesting that two ionizable groups, with p $K_a$  values of  $7.9 \pm 0.4$  and  $8.1 \pm 0.4$  for HpAgD,  $6.8 \pm 0.2$  and  $9.4 \pm 0.3$  for PgAgD, and  $6.1 \pm 0.2$  and  $9.2 \pm 0.3$  for SmAgD, contribute to substrate capture; effects on substrate capture include all steps (both substrate binding and transition state formation) up to and including the first irreversible step of the reaction. Note that deiminase activity was linear with respect to time over the entire pH range studied, thereby indicating that the loss of activity is not due to a non-specific effect on enzyme stability.

The plots of log  $k_{\text{cat}}$  versus pH were also bell-shaped for PgAgD and SmAgD with a pH optimum of ~8.0 (Figure 2), suggesting that two ionizable groups contribute to the rate liming step of the reaction. The p $K_a$  values obtained from this analysis are  $6.8 \pm 0.2$  and  $9.2 \pm 0.2$  for PgAgD, and,  $6.1 \pm 0.1$  and  $9.4 \pm 0.2$  for SmAgD. In contrast to PgAgD and

SmAgD, the plot of log  $k_{\text{cat}}$  versus pH for HpAgD fits well to a model in which only one ionizable contributes to the rate limiting step (p $K_a = 7.2 \pm 0.2$ , slope = 0.7  $\pm 0.2$ ).

#### **Solvent Isotope Effects**

pD profiles were also generated for HpAgD by measuring the steady state kinetic parameters in > 95% D<sub>2</sub>O. For HpAgD, plots of pL versus log  $k_{\rm cat}/K_{\rm m}$  and log  $k_{\rm cat}$  in H<sub>2</sub>O and D<sub>2</sub>O are bell-shaped and sigmoidal, respectively (Figure. 3). The solvent isotope effects (SIE) were also examined for HpAgD and SmAgD at the pH optimum. The results indicate that with respect to  $k_{\rm cat}/K_{\rm m}$  the reaction rate is faster in D<sub>2</sub>O for both enzymes ( $k_{\rm cat}/K_{\rm m}^{\rm H}/k_{\rm cat}/K_{\rm m}^{\rm D} = 0.71 \pm 0.30$  for HpAgD and  $k_{\rm cat}/K_{\rm m}^{\rm H}/k_{\rm cat}/K_{\rm m}^{\rm D} = 0.44 \pm 0.11$  for SmAgD). With respect to  $k_{\rm cat}$ , an inverse SIE was observed for HpAgD, whereas for SmAgD the SIE was normal. The SIE values are:  $k_{\rm cat}^{\rm H}/k_{\rm cat}^{\rm D} = 0.62$  and  $k_{\rm cat}^{\rm H}/k_{\rm cat}^{\rm D} = 1.05$  for HpAgD and SmAgD respectively.

Such inverse SIEs can be caused by medium effects, the dissociation of a metal chelated water, viscosity effects, or effects on thiol ionization (34). Although we cannot exclude medium effects as possible cause of the inverse SIE, these are typically small and normally discounted (34). Additionally, given that there are no metal ions required for catalysis and the viscosity effect is near zero (see below), the inverse SIE is most likely due to effects on thiol ionization; the fractionation factor of a thiol in  $D_2O$  is  $\sim 0.5$ , which results in an increased concentration of the thiolate species in  $D_2O$  (35). Given that the magnitude of these inverse SIEs on  $k_{\rm cat}/K_{\rm m}$  is similar to the fractionation factor of a thiol in  $D_2O$ , this data suggests that the enhanced reactivity of HpAgD and SmAgD in  $D_2O$  is due to the higher concentration of the reactive thiolate, i.e. an equilibrium SIE. Similar inverse SIEs on  $k_{\rm cat}/K_{\rm m}$  have been observed for other guanidinium modifying enzymes, e.g., PADs 1 and 4 (28,29), as well as other thiol containing enzymes, e.g. papain (36).

#### **Solvent Viscosity**

Solvent viscosity experiments were also performed to aid the characterization of AgD catalysis. For these experiments, the steady-state kinetic parameters were measured in assay buffers containing various concentrations of glycerol. The slopes obtained from plots of relative viscosity versus relative  $k_{\text{cat}}/K_{\text{m}}$  or relative  $k_{\text{cat}}$  are near zero for all of the enzymes tested (Table 1; see Figure 4 for representative data obtained with HpAgD). This lack of a solvent viscosity effect on  $k_{\text{cat}}$  and  $k_{\text{cat}}/K_{\text{m}}$  indicates that product release and substrate binding, respectively, are not rate limiting.

#### **lodoacetamide inactivation kinetics**

To determine the  $pK_a$  of the active site cysteine in HpAgD and SmAgD, the rates of iodoacetamide induced enzyme inactivation were determined as a function of time over a pH range of 7.0 to 9.25 (little to no inactivation was observed at lower pH values). For HpAgD, product formation was plotted versus time and then fit to a single exponential decay to determine the pseudo-first-order rate constants of iodoacetamide inactivation, i.e.  $k_{obs}$  (Figure 5). For SmAgD, the  $k_{obs}$  was determined by generating progress curves in the absence and presence of increasing concentrations of iodoacetamide (not shown). The second order rate constants for iodoacetamide inactivation, i.e.  $k_{inact}/K_I$ , were then obtained from the slopes of the plots of  $k_{obs}$  versus iodoacetamide concentration (Figure 5C). This process was repeated over the entire pH range and the  $k_{inact}/K_I$  values plotted as a function of pH. As depicted in Figure 6,  $k_{inact}/K_I$  increases with pH and fits to equation 6 are consistent with a single ionizable group with a p $K_a$  of 9.2  $\pm$  0.3 for HpAgD and 9.6  $\pm$  0.3 for SmAgD. Given that the p $K_a$  values are so high, it was not technically feasible to observe a plateau in the titration curves. Therefore, these values should be considered lower limits. Nevertheless, these data along with the pH profiles indicate that both HpAgD and SmAgD,

like other guanidinium modifying enzymes (6,27-29), possess a high p $K_a$  active site thiol. Note that substrate protection experiments are consistent with the modification of an active site residue (Figure 5A).

#### 2-chloroacetamidine inactivation kinetics

 $pK_a$  measurements with 2-chloroacetamidine were also performed to evaluate whether the positively charged nature of this compound could depress the  $pK_a$  of the active site cysteine by mimicking the effect of the positively charged guanidinium group in agmatine. Inactivation experiments were performed analogously to those described above for iodoacetamide. Representative plots of product formation versus time are depicted in Figure 7 for HpAgD. For HpAgD, plots of  $k_{obs}$  versus 2-chloroacetamidine concentration were hyperbolic (Figure 7C), thereby suggesting saturatable kinetics.  $k_{\text{inact}}/K_{\text{I}}$  values were obtained by fitting the observed data to equation 9. Subsequent plots of  $k_{\text{inact}}/K_{\text{I}}$  versus pH and kinact versus pH were then generated by repeating these experiments over the entire pH range. As depicted in Figure 8,  $k_{\text{inact}}/K_{\text{I}}$  increases as a function of pH and suggest that the p $K_a$  value of Cys324 in the free enzyme is 9.8  $\pm$  0.1. This value is in reasonable agreement with the descending limb of the pH versus  $k_{cat}/K_m$  rate profiles.  $k_{inact}$  also increases as a function of pH and displays a p $K_a$  of 9.3  $\pm$  0.5 (Figure 8C). For SmAgD, plots of residual activity versus 2-chloroacetamide concentration were linear over the range of 2chloroacetamidine concentrations tested. Plots of  $k_{\text{inact}}/K_{\text{I}}$  versus pH were then generated by performing the same experiments described above over the entire pH range and a p $K_a$  value of  $8.8 \pm 0.1$  was determined (Figure 8C). This value is also in reasonable agreement with the p $K_a$  corresponding to the descending limb of the pH versus  $k_{cat}/K_m$  rate profile (i.e., 9.2 ± 0.3). The data for both HpAgD and SmAgD indicate that the positive charge of the inactivation does not depress the  $pK_a$  of the active site thiol to an appreciable extent. Note that substrate protection experiments were performed to ensure that the inactivation was due to the modification of an active site residue (see Figure 7A for representative data obtained with HpAgD).

# IC<sub>50</sub> data with SmAgD and PgAgD

Previously, we reported that ABFA and ABCA (IC $_{50}$  = 6.8 and 0.87  $\mu$ M, respectively) are potent, mechanism based inactivators of HpAgD that covalently modify the active site thiolate, i.e. Cys324 (19). In order to determine if ABFA and ABCA inhibit all the AgDs, IC $_{50}$  values were measured for SmAgD and PgAgD (Table 2). Although the fact that the IC $_{50}$  values for SmAgD are significantly more potent than those obtained for either HpAgD and PgAgD, these results indicate that ABFA and ABCA are *pan* AgD inhibitors.

#### ABFA inhibition experiments of SmAgD

ABFA and ABCA likely inactivate the AgDs through one of at least two possible mechanisms (Figure 9A and 9B). The first mechanism involves the simple displacement of the halide in a  $S_N2$  manner. In the second mechanism, the active site thiolate attacks the iminium carbon, forming a tetrahedral intermediate. The sulfur then displaces the halide to form a three-membered sulfonium ring, which collapses to form the inactivated thioether. In order to characterize the mechanism by which ABFA inactivates SmAgD, the rates of inactivation for SmAgD were determined as a function of pH. Note that these studies focused only on SmAgD because this enzyme displays significantly higher rates of catalysis than either HpAgD or PgAgD, and it thus better behaved. As seen in Figure 10, the plots of  $k_{inact}/K_I$  versus pH are bell-shaped suggesting that two ionizable groups are critical for inactivator capture. Unfortunately, inactivator saturation was observed only at the pH optimum and  $k_{inact}$  versus pH rate profiles could not be generated. Nevertheless, the data are consistent with data obtained for the F- and Cl-amidine induced inactivation of PAD4, i.e., the  $k_{inact}/K_I$  versus pH rate profiles are also bell-shaped (37). Based on additional SIE,

proton inventory and  $k_{inact}$  versus pH rate profiles, this data indicated that general acid catalysis plays a critical role in the inactivation of PAD4, and further suggested that proton donation stabilizes the tetrahedral intermediate to facilitate the intramolecular displacement of the halide (Figure 9C). Given the similarities in the  $k_{inact}/K_I$  pH rate profiles, ABFA likely inactivates SmAgD via a similar mechanism.

# **Discussion**

Numerous GME family members are associated with human disease and/or represent potential therapeutic targets for giardiasis (e.g., ADI), bacterial infections (e.g., ADIs and AgDs), and cancer, RA, and colitis (e.g., PADs). To gain insights into the common features, and potential differences, in the catalytic mechanisms of the GME hydrolases that could be used to aid inhibitor development we, and others, have examined the catalytic mechanism of several PADs, DDAHs, ADIs, and AgDs (6,27–29,38). Based on these studies, a generally accepted catalytic mechanism has been proposed. In this mechanism, Asp84 and Asp204 likely play critical roles in binding and orienting the substrate guanidinium for nucleophilic attack by the side chain thiolate of Cys324 (Figure 11, HpAgD numbering). His202 would then be expected to act as a general acid, donating a proton to the departing amine either during the initial formation of the developing tetrahedral intermediate or after its collapse. His202 would then switch roles and act as a general base to activate a water molecule for nucleophilic attack and subsequent hydrolysis of the thiouronium intermediate generated in the previous step. Several aspects of this mechanism have been verified including the existence of the thiouronium intermediate in ADI and DDAH, as well as the key roles that the Asp groups, His, and Cys play in substrate recognition and activation, general acid/base catalysis, and covalent catalysis, respectively (6,27,38).

One issue regarding the mechanism that has drawn considerable debate is the protonation state of the active site Cys prior to substrate binding and how to reconcile the high  $pK_a$  of the thiol (27–29,39,40). Specifically, Fast and colleagues have suggested that DDAH utilizes a substrate assisted mechanism; the substrate binds to the thiol form of the enzyme and the positive charge of the guanidinium depresses the thiol  $pK_a$  such that the thiol proton is donated to solvent or an unknown base (Scheme 1). It is undoubtedly true that once bound, the proximity of the guanidinium to the thiol would decrease its  $pK_a$  by  $\geq 2.8$  pH units, as Fast and colleagues have shown using a reversible DDAH substrate analog (27). However, it is unclear whether this mechanism is universally used by all GME hydrolases and/or whether it is the kinetically preferred pathway. Along those lines, we have suggested that the PADs utilize a reverse protonation mechanism, in which only a small amount of the enzyme exists as the nucleophilic thiolate and that substrate binds preferentially, but not exclusively, to the thiolate form of the enzyme (28,29).

To both further our understanding of GME hydrolase catalysis and guide the design of inhibitors targeting the AgDs, we set out to characterize the mechanism of AgD catalysis. The HpAgD, SmAgD, and PgAgD  $k_{cat}/K_m$  pH profiles are bell-shaped indicating that there are two ionizable residues that are important for substrate capture. For SmAgD and PgAgD, the  $k_{cat}$  versus pH profiles are also bell-shaped, suggesting that two ionizable groups must be correctly protonated to achieve the maximum rate of hydrolysis. Based on previous precedents, these two ionizable groups likely correspond to the active site His and Cys (27,28). Surprisingly, the  $k_{cat}$  versus pH profiles for HpAgD is sigmoidal. This data indicates that only one proton transfer event is rate limiting for this enzyme and could either suggest that the catalytic mechanism used by HpAgD is different than the one utilized by SmAgD and PgAgD, or, more likely, that the rate limiting steps of the reaction differ between these enzymes. Given that HpAgD also exhibits an inverse SIE on  $k_{cat}$ , but no

solvent viscosity effect, the simplest interpretation of the data is that nucleophilic attack on the substrate guanidinium is rate limiting for HpAgD, but not for SmAgD or PgAgD.

In order to determine whether the Cys or the His corresponds to the ascending or descending limbs of the pH rate profiles,  $pK_a$  measurements were performed on the active site thiolate. This was accomplished by measuring the rate of inactivation of HpAgD and SmAgD over a range of pH values with iodoacetamide. Based on these experiments, the  $pK_a$  values of the active site Cys residue in HpAgD and SmAgD are 9.2 and 9.6, respectively, thereby suggesting that the  $pK_a$  of this Cys residue corresponds to the descending limb of the  $k_{cat}/K_m$  pH profile. As such, the ascending limb of the  $k_{cat}/K_m$  versus pH profile likely corresponds to the protonation state of the His. Given that these  $pK_a$  assignments are the reverse of the simplest assumption, i.e. that the rate of the reaction would increase as the thiolate concentration is increased, this data suggests that the AgDs, like the PADs, utilize what is commonly referred to as a reverse protonation mechanism; the term reverse protonation is used because it is the reverse of the simplest assumption (41,42). In such a mechanism, only a small fraction of the enzyme exists in the correct protonation state, i.e. the thiolate form, at the pH optimum (28,29,41,42).

For a thiol containing enzyme, one prediction of a reverse protonation mechanism is that an inverse SIE will be apparent on  $k_{cat}/K_m$ . This is the case because the fractionation factor of a thiol in  $D_2O$  is ~0.5, which results in an up to 2-fold increase in the concentration of the reactive thiolate in  $D_2O$  (35). Given that the magnitude of these inverse SIEs on  $k_{cat}/K_m$  are similar to the fractionation factor of a thiol in  $D_2O$ , this data suggests that the higher rate likely reflects an equilibrium proton transfer to solvent that generates a higher fraction of the more reactive thiolate. Note that similar inverse SIEs on  $k_{cat}/K_m$  have been observed for other active site thiol containing enzymes, including the guanidinium modifying enzymes PADs 1 and 4 (28,29) as well as papain (36). In contrast, for a pure substrate assisted mechanism a normal SIE would be expected because binding to the thiol form of the enzyme is obligatory, thus the lower concentration of the thiol in  $D_2O$ , would be expected to have either no effect or decrease  $k_{cat}/K_m$ .

To further differentiate between a reverse protonation mechanism and a substrate assisted mechanism, we evaluated whether the positively charged nature of 2-chloroacetamidine could depress the  $pK_a$  of the active site cysteine by mimicking the effect of the positively charged guanidinium group in agmatine. The results of these studies indicate that the positive charge has only a modest influence on the  $pK_a$  of the active site Cys; the  $pK_a$  values obtained with 2-chloroacetamidine (9.8 and 8.8) are similar to those obtained (9.2 and 9.6) with iodoacetamide for HpAgD and SmAgD, respectively. Although it is unclear how well 2-chloroacetamidine mimics a true substrate, the fact that this positively charged inactivator does not markedly depress the measured  $pK_a$  values further argues against the obligatory binding of the inactivators, and by extension the substrate, to the thiol form of the enzyme as would occur in a "pure" substrate assisted mechanism (Scheme 1).

Given that the rates of 2-chloroacetamidine inactivation for HpAgD displayed saturable kinetics; it was also possible to obtain a  $pK_a$  value from the  $k_{inact}$  versus pH rate profile (the measured  $pK_a$  is 9.3). The fact that this  $pK_a$  is similar to the value obtained from the  $k_{inact}/K_I$  versus pH rate profile (i.e., 9.3 versus 9.8, respectively) indicates that the positive charge of the inactivator only modestly depresses the  $pK_a$  of the active site Cys. As such, this data is also inconsistent with the "pure" substrate assisted mechanism because the kinetically preferred pathway suggests that thiolate deprotonation from the reactive species is not required for catalysis.

#### Conclusions

pH rate profiles,  $pK_a$  inactivation, and solvent isotope experiments suggest that, like the PADs, the AgDs preferentially utilize a reverse protonation mechanism, and not a 'pure' substrate assisted mechanism. These studies will undoubtedly aid our future efforts to develop inhibitors targeting the AgDs.

#### **ABBREVIATIONS**

AgDagmatine deiminaseNCPN-carbamoyl putrescinePADprotein arginine deiminase

Cit citrulline

**BAAE** benzoyl L-arginine ethyl ester benzoyl L-arginine amide

**DTT** dithiothreitol

**GST** glutathione S-transferase

**TCEP** Tris(2-carboxyethyl)phosphine hydrochloride

**HEPES** N-(2-hydroxyethyl)piperazine-N'-(2-ethanesulfonic acid)

**Orn** Ornithine

**ABFA** *N*-(4-aminobutyl)-2-fluoro-ethanimidamide **ABCA** *N*-(4-aminobutyl)-2-chloro-ethanimidamide

#### References

- Linsky T, Fast W. Mechanistic similarity and diversity among the guanidine-modifying members of the pentein superfamily. Biochim Biophys Acta. 2010; 1804:1943–1953. [PubMed: 20654741]
- Shalev-Alon G, Sukenik A, Livnah O, Schwarz R, Kaplan A. A novel gene encoding amidinotransferase in the cylindrospermopsin producing cyanobacterium Aphanizomenon ovalisporum. FEMS Microbiol Lett. 2002; 209:87–91. [PubMed: 12007659]
- 3. Tran CT, Leiper JM, Vallance P. The DDAH/ADMA/NOS pathway. Atheroscler Suppl. 2003; 4:33–40. [PubMed: 14664901]
- Boger RH. Asymmetric dimethylarginine, an endogenous inhibitor of nitric oxide synthase, explains the "L-arginine paradox" and acts as a novel cardiovascular risk factor. J Nutr. 2004; 134:2842S– 2847S. discussion 2853S. [PubMed: 15465797]
- Leiper J, Nandi M, Torondel B, Murray-Rust J, Malaki M, O'Hara B, Rossiter S, Anthony S, Madhani M, Selwood D, Smith C, Wojciak-Stothard B, Rudiger A, Stidwill R, McDonald NQ, Vallance P. Disruption of methylarginine metabolism impairs vascular homeostasis. Nat Med. 2007; 13:198–203. [PubMed: 17273169]
- 6. Li Z, Kulakova L, Li L, Galkin A, Zhao Z, Nash TE, Mariano PS, Herzberg O, Dunaway-Mariano D. Mechanisms of catalysis and inhibition operative in the arginine deiminase from the human pathogen Giardia lamblia. Bioorg Chem. 2009; 37:149–161. [PubMed: 19640561]
- 7. Glazer ES, Piccirillo M, Albino V, Di Giacomo R, Palaia R, Mastro AA, Beneduce G, Castello G, De Rosa V, Petrillo A, Ascierto PA, Curley SA, Izzo F. Phase II Study of Pegylated Arginine Deiminase for Nonresectable and Metastatic Hepatocellular Carcinoma. J Clin Oncol. 2010
- Jones JE, Causey CP, Knuckley B, Slack-Noyes JL, Thompson PR. Protein arginine deiminase 4 (PAD4): Current understanding and future therapeutic potential. Curr Opin Drug Discov Devel. 2009; 12:616–627.

 Sakakibara Y, Yanagisawa H. Agmatine deiminase from cucumber seedlings is a mono-specific enzyme: purification and characteristics. Protein Expr Purif. 2003; 30:88–93. [PubMed: 12821325]

- Baumann S, Sander A, Gurnon JR, Yanai-Balser GM, Van Etten JL, Piotrowski M. Chlorella viruses contain genes encoding a complete polyamine biosynthetic pathway. Virology. 2007; 360:209–217. [PubMed: 17101165]
- Griswold AR, Jameson-Lee M, Burne RA. Regulation and physiologic significance of the agmatine deiminase system of Streptococcus mutans UA159. J Bacteriol. 2006; 188:834

  [PubMed: 16428386]
- 12. Williams BJ, Du RH, Calcutt MW, Abdolrasulnia R, Christman BW, Blackwell TS. Discovery of an operon that participates in agmatine metabolism and regulates biofilm formation in Pseudomonas aeruginosa. Mol Microbiol.
- 13. Li G, Regunathan S, Barrow CJ, Eshraghi J, Cooper R, Reis DJ. Agmatine: an endogenous clonidine-displacing substance in the brain. Science. 1994; 263:966–969. [PubMed: 7906055]
- 14. Regunathan S, Reis DJ. Imidazoline receptors and their endogenous ligands. Annu Rev Pharmacol Toxicol. 1996; 36:511–544. [PubMed: 8725400]
- 15. Satriano J. Arginine pathways and the inflammatory response: interregulation of nitric oxide and polyamines: review article. Amino Acids. 2004; 26:321–329. [PubMed: 15290337]
- Joshi MS, Ferguson TB Jr, Johnson FK, Johnson RA, Parthasarathy S, Lancaster JR Jr. Receptor-mediated activation of nitric oxide synthesis by arginine in endothelial cells. Proc Natl Acad Sci U S A. 2007; 104:9982–9987. [PubMed: 17535904]
- Su CH, Liu IM, Chung HH, Cheng JT. Activation of I2-imidazoline receptors by agmatine improved insulin sensitivity through two mechanisms in type-2 diabetic rats. Neurosci Lett. 2009; 457:125–128. [PubMed: 19429177]
- Gobert AP, McGee DJ, Akhtar M, Mendz GL, Newton JC, Cheng Y, Mobley HL, Wilson KT. Helicobacter pylori arginase inhibits nitric oxide production by eukaryotic cells: a strategy for bacterial survival. Proc Natl Acad Sci U S A. 2001; 98:13844–13849. [PubMed: 11717441]
- Jones JE, Causey CP, Lovelace L, Knuckley B, Flick H, Lebioda L, Thompson PR. Characterization and inactivation of an agmatine deiminase from Helicobacter pylori. Bioorg Chem. 2010; 38:62–73. [PubMed: 20036411]
- Luo Y, Arita K, Bhatia M, Knuckley B, Lee YH, Stallcup MR, Sato M, Thompson PR. Inhibitors and inactivators of protein arginine deiminase 4: functional and structural characterization. Biochemistry. 2006; 45:11727–11736. [PubMed: 17002273]
- Luo Y, Knuckley B, Lee YH, Stallcup MR, Thompson PR. A fluoroacetamidine-based inactivator of protein arginine deiminase 4: design, synthesis, and in vitro and in vivo evaluation. J Am Chem Soc. 2006; 128:1092–1093. [PubMed: 16433522]
- 22. Luo Y, Knuckley B, Bhatia M, Pellechia PJ, Thompson PR. Activity-based protein profiling reagents for protein arginine deiminase 4 (PAD4): synthesis and in vitro evaluation of a fluorescently labeled probe. J Am Chem Soc. 2006; 128:14468–14469. [PubMed: 17090024]
- Causey CP, Thompson PR. An improved synthesis of haloaceteamidine-based inactivators of protein arginine deiminase 4 (PAD4). Tetrahedron Lett. 2008; 49:4383–4385. [PubMed: 19587776]
- 24. Stone EM, Schaller TH, Bianchi H, Person MD, Fast W. Inactivation of two diverse enzymes in the amidinotransferase superfamily by 2-chloroacetamidine: dimethylargininase and peptidylarginine deiminase. Biochemistry. 2005; 44:13744–13752. [PubMed: 16229464]
- 25. Wang Y, Hu S, Fast W. A click chemistry mediated in vivo activity probe for dimethylarginine dimethylaminohydrolase. J Am Chem Soc. 2009; 131:15096–15097. [PubMed: 19919155]
- 26. Li L, Li Z, Chen D, Lu X, Feng X, Wright EC, Solberg NO, Dunaway-Mariano D, Mariano PS, Galkin A, Kulakova L, Herzberg O, Green-Church KB, Zhang L. Inactivation of microbial arginine deiminases by L-canavanine. J Am Chem Soc. 2008; 130:1918–1931. [PubMed: 18205354]
- Stone EM, Costello AL, Tierney DL, Fast W. Substrate-assisted cysteine deprotonation in the mechanism of dimethylargininase (DDAH) from Pseudomonas aeruginosa. Biochemistry. 2006; 45:5618–5630. [PubMed: 16634643]

28. Knuckley B, Bhatia M, Thompson PR. Protein arginine deiminase 4: evidence for a reverse protonation mechanism. Biochemistry. 2007; 46:6578–6587. [PubMed: 17497940]

- Knuckley B, Causey CP, Jones JE, Bhatia M, Dreyton CJ, Osborne TC, Takahara H, Thompson PR. Substrate specificity and kinetic studies of PADs 1, 3, and 4 identify potent and selective inhibitors of protein arginine deiminase 3. Biochemistry. 2010; 49:4852–4863. [PubMed: 20469888]
- Griswold AR, Nascimento MM, Burne RA. Distribution, regulation and role of the agmatine deiminase system in mutans streptococci. Oral Microbiol Immunol. 2009; 24:79–82. [PubMed: 19121075]
- Kearney PL, Bhatia M, Jones NG, Yuan L, Glascock MC, Catchings KL, Yamada M, Thompson PR. Kinetic characterization of protein arginine deiminase 4: a transcriptional corepressor implicated in the onset and progression of rheumatoid arthritis. Biochemistry. 2005; 44:10570– 10582. [PubMed: 16060666]
- 32. Knipp M, Vasak M. A colorimetric 96-well microtiter plate assay for the determination of enzymatically formed citrulline. Anal Biochem. 2000; 286:257–264. [PubMed: 11067748]
- 33. Leatherbarrow, RJ. Grafit Ver 5.0. Erathicus Software; Staines, UK: 2004.
- 34. Karsten WE, Lai CJ, Cook PF. Inverse Solvent Isotope Effects in the Nad-Malic Enzyme Reaction Are the Result of the Viscosity Difference between D2o and H2o Implications for Solvent Isotope Effect Studies. Journal of the American Chemical Society. 1995; 117:5914–5918.
- 35. Quinn, DM.; Sutton, LD. Theoretical basis and mechanistic utility of solvent isotope effects. In: Cook, PF., editor. Enzyme Mechanism from Isotope Effects. CRC Press; Boca Raton, FL: 1991. p. 73-126.
- 36. Lewis SD, Johnson FA, Shafer JA. Effect of cysteine-25 on the ionization of histidine-159 in papain as determined by proton nuclear magnetic resonance spectroscopy. Evidence for a his-159-Cys-25 ion pair and its possible role in catalysis. Biochemistry. 1981; 20:48–51. [PubMed: 7470479]
- 37. Knuckley B, Causey CP, Pellechia PJ, Cook PF, Thompson PR. Haloacetamidine-based inactivators of protein arginine deiminase 4 (PAD4): evidence that general acid catalysis promotes efficient inactivation. Chembiochem. 2010; 11:161–165. [PubMed: 20014086]
- 38. Galkin A, Lu X, Dunaway-Mariano D, Herzberg O. Crystal structures representing the Michaelis complex and the thiouronium reaction intermediate of Pseudomonas aeruginosa arginine deiminase. J Biol Chem. 2005; 280:34080–34087. [PubMed: 16091358]
- 39. Ke Z, Wang S, Xie D, Zhang Y. Born-Oppenheimer ab initio QM/MM molecular dynamics simulations of the hydrolysis reaction catalyzed by protein arginine deiminase 4. J Phys Chem B. 2009; 113:16705–16710. [PubMed: 20028143]
- 40. Ke Z, Zhou Y, Hu P, Wang S, Xie D, Zhang Y. Active site cysteine is protonated in the PAD4 Michaelis complex: evidence from Born-Oppenheimer ab initio QM/MM molecular dynamics simulations. J Phys Chem B. 2009; 113:12750–12758. [PubMed: 19507815]
- 41. Frankel BA, Kruger RG, Robinson DE, Kelleher NL, McCafferty DG. Staphylococcus aureus sortase transpeptidase SrtA: insight into the kinetic mechanism and evidence for a reverse protonation catalytic mechanism. Biochemistry. 2005; 44:11188–11200. [PubMed: 16101303]
- 42. Mock WL, Stanford DJ. Anisylazoformylarginine: a superior assay substrate for carboxypeptidase B type enzymes. Bioorg Med Chem Lett. 2002; 12:1193–1194. [PubMed: 11934586]

**Figure 1.** Agmatine metabolism in bacteria. Pathway A: Agmatine, **1**, is converted to *N*-Carbamoylputrescine (NCP), **2**, and NH<sub>3</sub> by agmatine deiminase (AgD). For *S. mutans*, **2** is converted into putrescine, **3**, by putrescine transcarbamoylase (PTC). Pi reacts with carbamoyl to form carbamoylphosphate, **4**, which gets degraded to ATP, NH<sub>3</sub>, and CO<sub>2</sub> by carbamate kinase (CK). Pathway B: For *H. pylori*, and *P. gingivalis*, **2** is converted to **3** by NCP amidohydrolase (NCPA), NH<sub>3</sub>, and CO<sub>2</sub>.

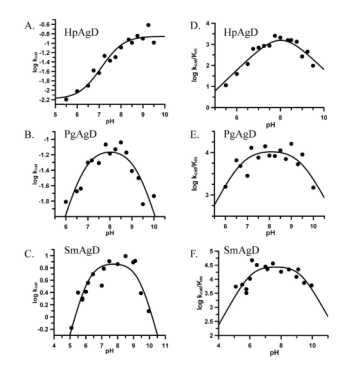


**Figure 2.** log  $k_{\text{cat}}$  versus pH rate profiles for (**A**) HpAgD, (**B**) PgAgD, and (**C**) SmAgD. log  $k_{\text{cat}}$ /K<sub>m</sub> versus pH rate profiles for (**D**) HpAgD, (**E**) PgAgD, and (**F**) SmAgD.

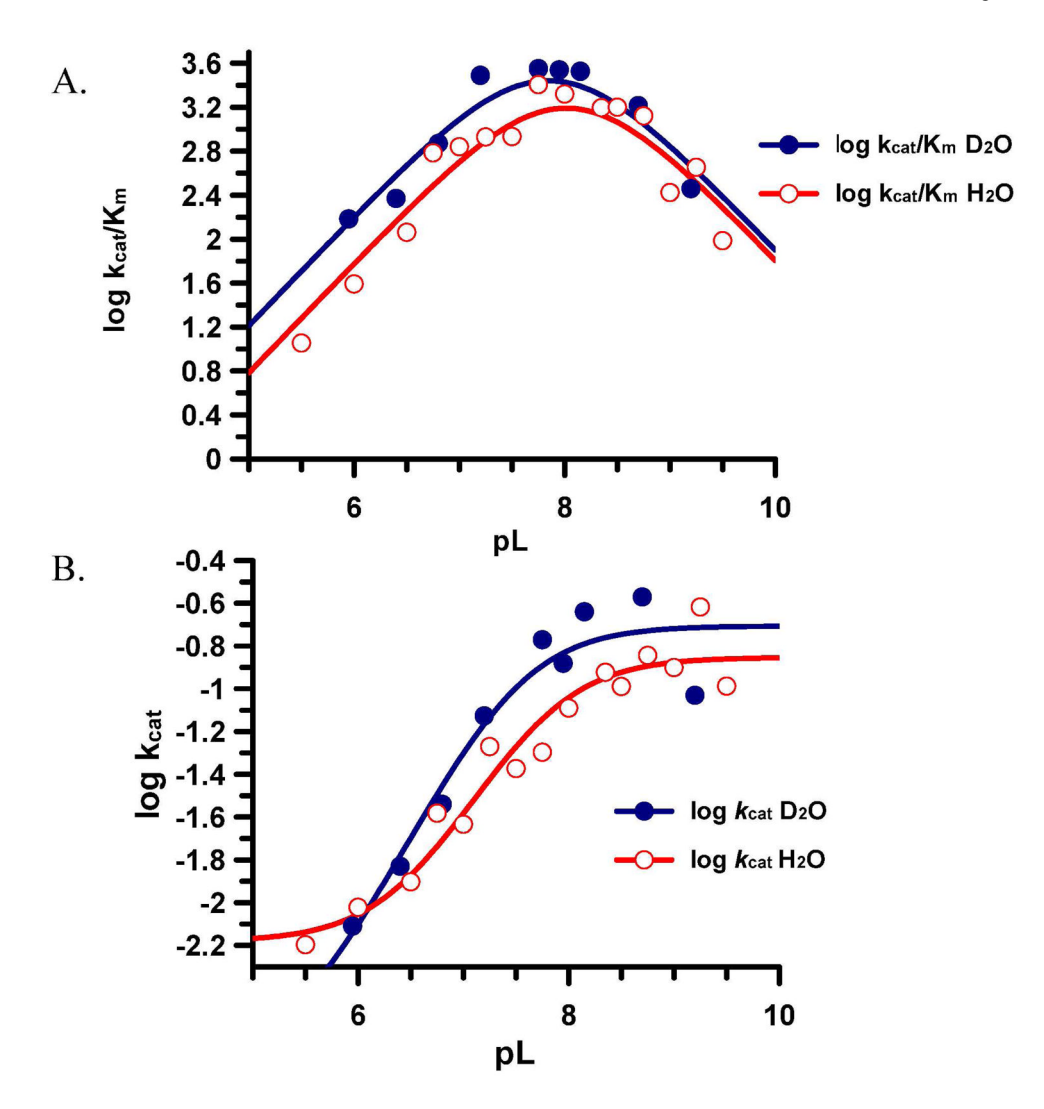


**Figure 3.** Solvent isotope effect for HpAgD. (**A**) plot of  $\log k_{cat}/K_m$  versus pH in H<sub>2</sub>O (red) and D<sub>2</sub>O (blue). (**B**) plot of  $\log k_{cat}$  versus pH in H<sub>2</sub>O (red) and D<sub>2</sub>O (blue).

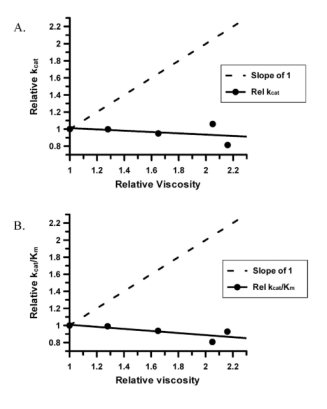


Figure 4. Solvent viscosity effect for HpAgD. (A) plot of relative viscosity versus relative  $k_{cat}$ . (B) plot of relative viscosity versus relative  $k_{cat}/K_m$ .

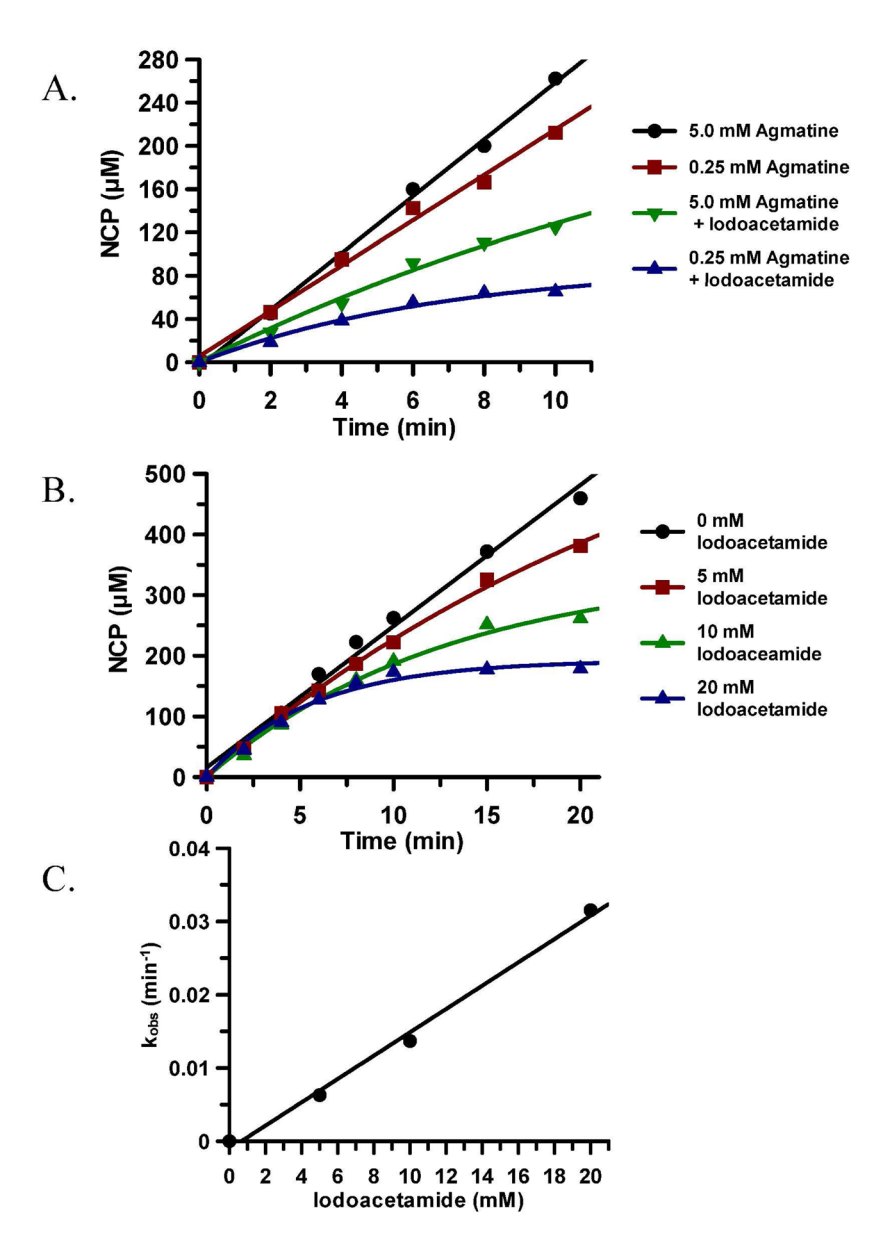
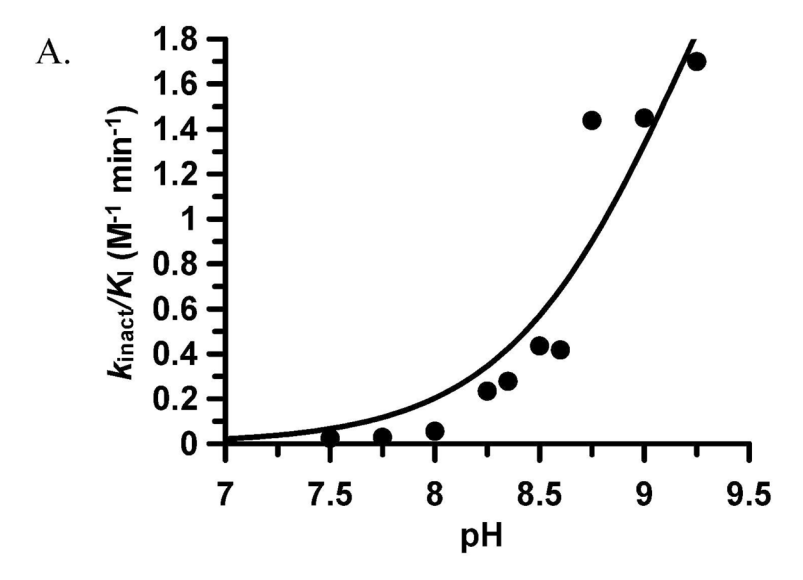
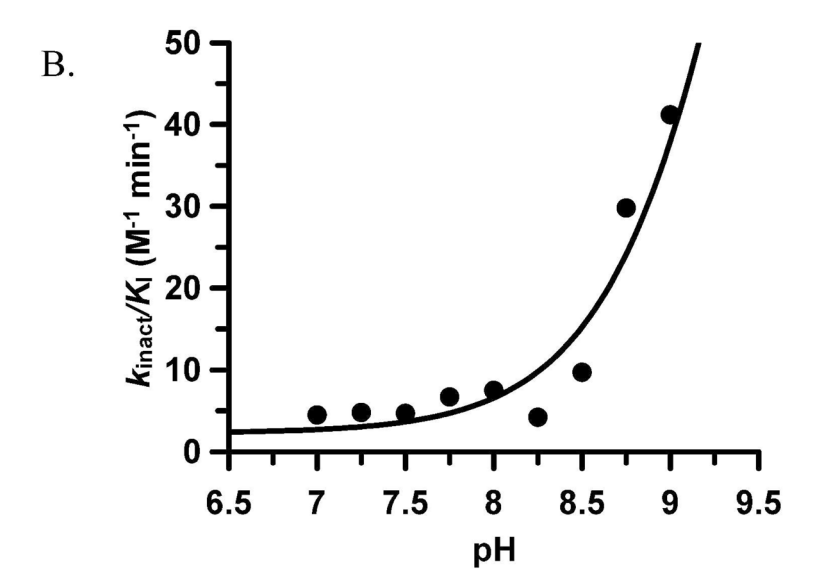
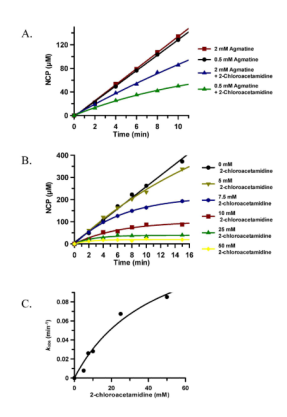


Figure 5. (A) Iodoacetamide inactivation experiments for HpAgD. (A) Substrate protection experiment. (B) Progress curves with increasing concentrations of iodoacetamide. (C) Plot of  $k_{\rm obs}$  versus concentration of iodoacetamide.





**Figure 6.**  $k_{\text{inact}}/K_{\text{I}}$  values obtained from iodoacetamide inactivation experiments were plotted versus pH for HpAgD (**A**) and SmAgD (**B**).



**Figure 7.** 2-chloroacetamidine inactivation experiments. (**A**) Substrate protection experiment for HpAgD. (**B**) Progress curves with increasing concentrations of 2-chloroacetamidine. (**C**) Plot of  $k_{\text{obs}}$  versus concentration of 2-chloroacetamidine.

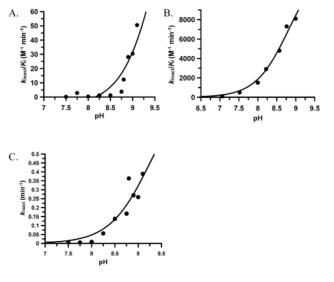


**Figure 8.** pH dependence of 2-chloroacetamidine inactivation. (**A**) Plot of  $k_{\text{inact}}/K_{\text{I}}$  versus pH obtained with HpAgD. (**B**) Plot of  $k_{\text{inact}}$  versus pH obtained with HpAgD. (**C**) Plot of  $k_{\text{inact}}/K_{\text{I}}$  versus pH obtained with SmAgD.

Figure 9.

Three possible mechanisms of inactivation for ABFA and ABCA. (A)  $S_N2$  displacement of the halide. (B) A multistep mechanism wherein the active site thiolate attacks the imminium carbon to form a tetrahedral intermendiate. This intermediate rearranges to form a 3-membered sulfonium ring, which collapses to form the inactivated thioether moiety. (C) A multistep mechanism involving general acid catalysis to stabilize the intial tetrahedral intermediate.

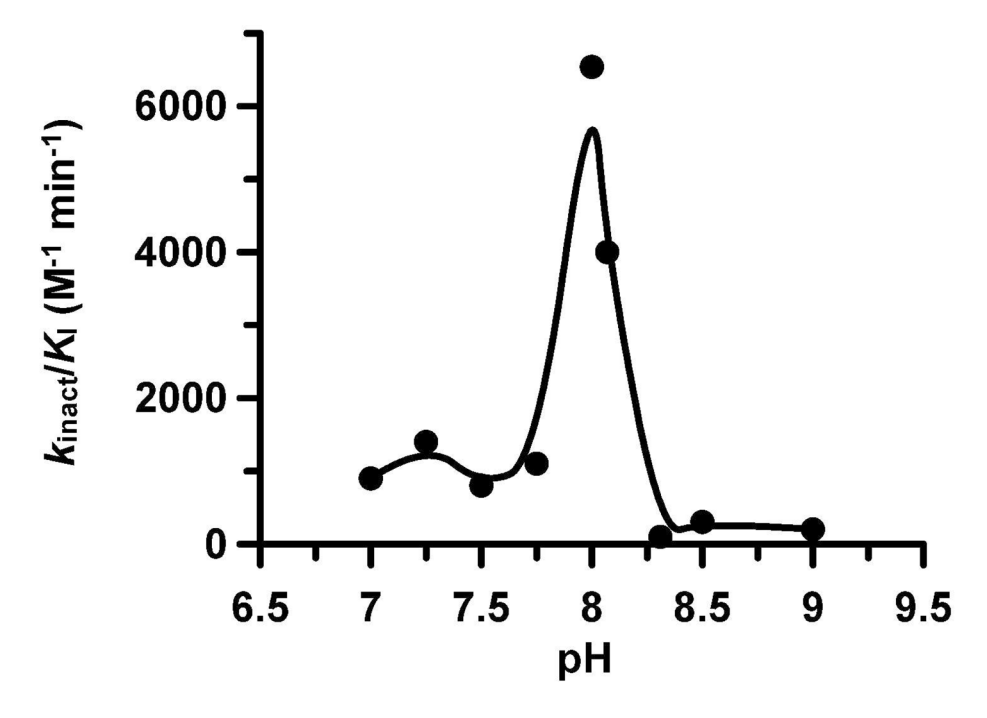


Figure 10. ABFA inactivation kinetics. Plot of  $k_{\text{inact}}/K_{\text{I}}$  versus pH ABFA obtained with SmAgD.

Figure 11.

Mechanism of AgD catalysis (HpAgD numbering). The active site thiolate attacks the guanidinium carbon and the histidine acts as a general acid to donate a proton to the departing amine. The tetrahedral intermediate collapses to form the S-alkylthiouronium intermediate. Ammonia is exchanged for a molecule of water and the histidine acts as a general base, which activates the water molecule for nucleophilic attack. The second tetrahedral intermediate collapses to form the final product.

E-SH + I 
$$\xrightarrow{\beta K_{b}}$$
 E-SH • I

$$\downarrow K_{a} \qquad \qquad \downarrow \alpha K_{a}$$
H
+
+
E-S- + I  $\xrightarrow{K_{b}}$  E-S- • I  $\longrightarrow$  E-S — I

**Scheme 1.** Inactivator binding to E-SH (upper) or E-S<sup>-</sup> (lower).

Table 1

# Solvent viscosity effect.

	SmAgD	HpAgD
Slope of relative viscosity versus relative $k_{\rm cat}$	$0.22 \pm 0.20$	-0.08 ± 0.10
Slope of relative viscosity versus relative $k_{\rm cat}/K_{\rm m}$	-0.12 ± 0.14	$-0.12 \pm 0.06$

# Table 2

# Summary of $IC_{50}$ values

Inhibitor	HpAgD (µM)	SmAgD (µM)	PgAgD (µM)
ABFA	$6.8 \pm 0.26$	$0.27 \pm 0.10$	91 ± 25
ABCA	$0.87 \pm 0.03$	$0.26 \pm 0.61$	$15 \pm 3$